

Paper:

Study of Multirate Sampled Acquisition of Lightning Current Waveform Based on Short-Time Fourier Transform

Xing Jin*, Dian Zhang*, Jingjing Zhang*, and Yuan Feng**

*School of Automation, China University of Geosciences

Wuhan 430073, China

E-mail: {jinxing, work.zhang}@cug.edu.cn, 1335442725@qq.com

**School of International Education, Changchun Institute of Technology

Changchun 130012, China

[Received July 7, 2016; accepted October 23, 2016]

In the field of lightning current waveform acquisition, since the lightning stroke signal contains continuous current whose change is relatively flat, sampling with a fixed frequency is a waste of memory resources, and may even increase system design difficulty and cost. The multirate sampled method has been proposed to acquire lightning current waveforms based on the short-time Fourier transform (STFT) to counter this problem and cubic Hermite interpolation has been used to optimize sampled data. The results of simulation and lightning experiments have shown that the multirate sampled method reduces memory resource consumption by at least 70% and ensures high accuracy. The feasibility and effectiveness of the multirate sampled method have also been confirmed.

Keywords: lightning current waveform, short-time Fourier transform, multirate sampled method, cubic Hermite interpolation, memory resource

1. Introduction

Lightning, a high-intensity electromagnetic pulse phenomenon seen frequently in nature, has attracted extensive attentions among those working in meteorology, aerospace, electricity and electronics, petroleum, etc. [1]. The grid, which uses a geometry of up to thousands of kilometers and features wide-area distribution, is easily struck by lightning [2], so nations world-wide have taken numerous measures to avoid lightning strikes on substations and transmission lines. Due to transmission line flashovers caused by lightning strikes, however, power grid failures remain frequent [3,4]. Lightning disasters has become one of the three severest threats to safe power system operation, together with natural disasters and external damage [5]. Lightning current waveform and amplitudes of great importance to protection against lightning, remain a major threat to grid protection against lightning, as does a full understanding of lightning current on transmission lines [6]. This makes obtaining the precise amplitude and waveform of lightning current a key

technique in lightning protection.

The mainstream method of collecting lightning current amplitude and waveform is high-speed sampling at a fixed frequency using the Rogowski coil and high-speed A/D converters [6–8]. Depending on lightning's characteristics, regardless of the existence of high-frequency components, most current signals inside the wave change relatively smooth [9, 10]. To get full information, frequencies exceeding twice the highest lightning signal for sampling should be used based on the Nyquist theory [11]. This, however, creates large amounts of redundant data and wastes cache memory resources, even as it increases system design difficulty and cost [11]. It thus becomes necessary to reduce data redundancy while obtaining full information on lightning signals as precisely as possible.

In the sections that follow, we present a multirate sampled method based on short-time Fourier transforms. We began by analyzing the frequency distribution of typical lightning current signals by using the short-time Fourier transform and a multirate sampled method for sampling lightning stroke signals has been proposed based on the analysis results. Next, we completed the computer algorithm code. Then we used cubic Hermite interpolation to optimize sampled data. These efforts resulted in a flexible sample rate and a significant reduction in memory resource waste.

2. The Short-Time Fourier Transform and Piecewise Cubic Hermite Interpolation

2.1. Short-Time Fourier Transform

The Fourier transform is the bridge linking the time and frequency domains opening the door to frequency domain analysis. The discrete Fourier transform (DFT) and the inverse discrete Fourier transform (IDFT) are as follows:

$$X[k] = \sum_{n=0}^{N-1} x(n) e^{-j\frac{2\pi}{N}kn}, \quad k \in [0 \ N-1] \quad \dots \quad (1)$$

$$x[n] = \frac{1}{N} \sum_{k=0}^{N-1} X[k] e^{j\frac{2\pi}{N}kn}, \quad n \in [0 \ N-1] \quad \dots \quad (2)$$



The DFT was developed from the continuous Fourier transform (CFT) for further processing by the computer. As Eq. (1) shows, the Fourier transform only reflects the general signal characteristics of a signal in the whole time domain, and does not provide information on frequency in a partial time. In other words, it does not provide time orientation. This in turn implies that it is unfavorable for analyzing nonstationary signals. Gabor thus proposed the short-time Fourier transform in 1946, which assumes that the nonstationary signal is stationary in a short time. By transforming waveforms with the DFT, we learn local frequency information on the signal, which is intercepted by a sliding window function.

$$STFT_x(t, \Omega) = \left\langle x(\tau), g(\tau - t)e^{j\Omega\tau} \right\rangle = \int x(\tau)g^*(\tau - t)e^{-j\Omega\tau}d\tau \dots (3)$$

$$STFT_x(t, \Omega) = \frac{1}{2\pi} \left\langle X(\nu), G(\nu - \Omega)e^{j(\nu - \Omega)t} \right\rangle = \frac{1}{2\pi} \int X(\nu)G^*(\nu - \Omega)e^{j(\nu - \Omega)t}d\nu \dots (4)$$

The short-time Fourier transform is explained as follows: First, change time variable t of function $x(t)$ and $g(t)$ into τ . Next, intercept function $x(\tau)$ with window function $g(\tau)$ in a time domain, then use the DFT to get the intercepted signal frequency at time t . Move the center of window function $g(\tau)$ constantly and process the intercepted signal with the Fourier transform to get all of the frequencies of these intercepted signals. $STFT_x(t, \Omega)$ shown in Eq. (3), consists of these frequencies. Intercepting $x(\tau)$ with window function $g(\tau - t)$ in the time domain is equivalent to intercepting $X(\nu)$ with window function $G(\nu - \Omega)$ in the frequency domain, so $STFT_x(t, \Omega)$ may be rewritten as shown in Eq. (4). $STFT_x(t, \Omega)$ is thus a 2-D function of variables (t, Ω) [12, 13].

2.2. Piecewise Cubic Hermite Interpolation

Assuming that the values of function $f(x)$ are y_0, y_1 at x_0, x_1 and that the values of their first derivative are y'_0, y'_1 , the cubic Hermite interpolation is written as

$$H_3 = y_0\alpha_0(x) + y_1\alpha_1(x) + y'_0\beta_0(x) + y'_1\beta_1(x) \quad (5)$$

where

$$\alpha_0(x) = \left(1 + 2\frac{x - x_0}{x_1 - x_0}\right) \left(\frac{x - x_1}{x_0 - x_1}\right)^2$$

$$\alpha_1(x) = \left(1 + 2\frac{x - x_1}{x_0 - x_1}\right) \left(\frac{x - x_0}{x_1 - x_0}\right)^2$$

$$\beta_0(x) = (x - x_0) \left(\frac{x - x_1}{x_0 - x_1}\right)^2$$

$$\beta_1(x) = (x - x_1) \left(\frac{x - x_0}{x_1 - x_0}\right)^2$$

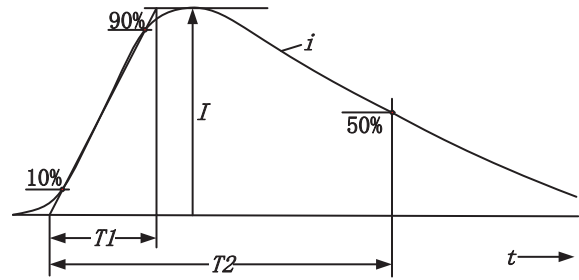


Fig. 1. Typical lightning strike waveform.

Table 1. Statistics of lightning currents.

| Parameter | Typical Value | Range |
|-----------------------------------------|---------------|--------|
| Peak current I [kA] | 20 | 2~200 |
| Average steepness I/T_1 [kA/ μ s] | 10 | 1~80 |
| Front time T_1 [μ s] | 2 | 1~30 |
| Time to half value T_2 [μ s] | 40 | 10~250 |

When function $f^{(4)}(x)$ exists and is continuous at $[x_0, x_1]$, the error of the interpolation is written in the form of

$$R_3 = \frac{f^{(4)}(\xi)}{4!} (x - x_0)^2 (x - x_1)^2, \quad x_0 \leq \xi \leq x_1 \quad (6)$$

As polynomial interpolation, cubic interpolation is high-order. The Runge phenomenon may occur as the order of interpolation rises, so for higher order interpolation, it is preferable to use piecewise cubic Hermite interpolation, which refers to interpolation between each two adjacent points with cubic Hermite interpolation [14].

3. Theoretical Analysis of System

3.1. Analysis of the Lightning Strike Signal

Based on the IEC standard, standard lightning-strike waveforms are of two types: the exponential wave and the square wave. Exponential waves are used to simulate a lightning strike in the laboratory [15]. **Fig. 1** shows a typical exponential lightning strike waveform used in tests. I is peak current, T_1 is front time, and T_2 is the time to the half value of the lightning current. As shown in **Fig. 1**, the lightning strike waveform consists of a wave front that is increasingly monotonous and whose wave tail decreases monotonously, and where wave front duration is significantly shorter less than that of the wave tail.

At present, lightning current parameters are not uniform, and most parameters have only a value range and statistics. **Table 1** shows statistics of lightning currents. Most lightning strikes have negative polarity and account for over 90% of the amount of lightning strikes. The peak current of about 95% of all strikes exceeds 80 kA. About 95% of strikes have a front time within 18 μ s, and about 95% have a time to half value that is within 200 μ s. Each

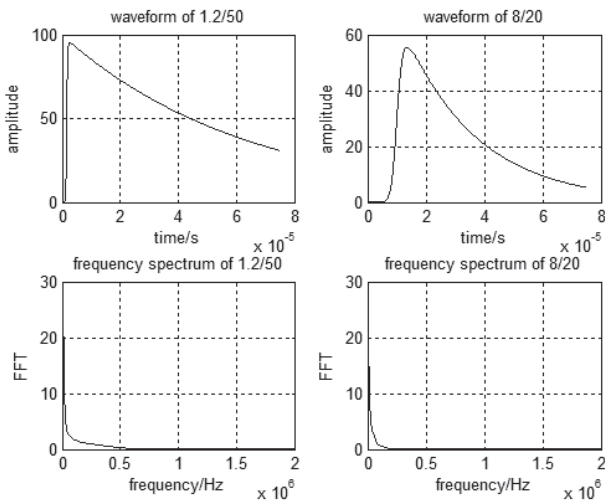


Fig. 2. Lightning current waves and their corresponding frequency spectra.

strike contains 2 or 3 return strikes and each pair of return strikes has a time interval ranging from 0.6 ms to 0.8 s. Most lightning strikes are within 800 ms [16–19].

3.2. Spectral Analysis of the Lightning Current

To facilitate theoretical forecasts and lightning current research, the IEC proposed an analytical exponential wave formula in 1995 [15, 20]:

$$i(t) = \frac{I_0}{h} \frac{\left(\frac{t}{\tau_1}\right)^{10}}{1 + \left(\frac{t}{\tau_1}\right)^{10}} e^{-\frac{t}{\tau_2}} \dots \dots \dots (7)$$

I_0 is the lightning current peak, h is the peak current correction coefficient, τ_1 is the wave front time constant, and τ_2 is the wave tail time constant. Common impulse current waves include 1.2/50 μ s, 8/20 μ s and 10/350 μ s. Waves of 10/350 μ s are specified as standard impulse currents used in protecting buildings against lightning. A value of 1.2/50 μ s is the lightning current waveform recommended and specified by the IEC, and waves of 8/20 μ s are used in testing that is stipulated by standards in China [5,6]. The following details against the first 2 types of IEC’s lightning waveforms to analyze their frequency spectrum.

Analyzing original sampling signals with the DFT shown in Eq. (1) yields the signal frequency spectrum. The original sampling signals and their corresponding frequency spectra are shown in **Fig. 2**. Note that lightning current frequencies are mainly distributed between 0 and 1 MHz, and most of their energy is concentrated between 0 and 500 KHz. Spectrum wave changes in exponent attenuation and signal amplitudes exceeding 1 MHz are far below the resolutions of most A/D converters.

To obtain lightning frequency spectrum distributions in individual periods, the signal should be transformed for its short-time Fourier transform using Eq. (3), the results

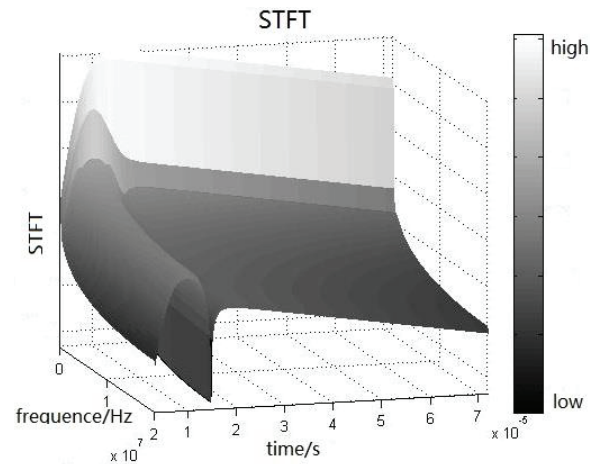


Fig. 3. Time-frequency distribution of lightning current waveforms.

of which are shown in **Fig. 3**. It can be inferred that low frequency components are basically throughout the whole time domain, and their energy change is relatively smooth. However, the great change has appeared in high frequency components with time. In the initial stage, amplitude rises in a concave curve. High-frequency components increase gradually and peak at the point of inflexion on a curve. The rising speed of amplitude then slows and the curve rises in a convex curve. High-frequency components then start to decrease and a blank space appears at the wave crest. The amplitude then gradually declines. The changing trends in high-frequency components are similar to that described previously, only at a much lower maximum frequency.

Time-frequency analysis shows that changing trends in high-frequency components are similar to those of the signal derivative of the lightning signal. There are more high-frequency components when the derivative is larger, and vice versa. Nevertheless, unlike with high frequencies, low-frequency components change relatively smoothly. If the sampling rate adaptively tracks the derivative of the lightning signal, the highest frequency in current sampling can be tracked, so we can find the most appropriate current sampling rate for reducing the number of sampling points, thus achieving the objective of decreasing data size.

3.3. The Design of Algorithm Code of Multirate Sampled Method

Sampling rates of the multirate sampled method are divided into 4 to 8 frequencies. For further computer processing and the optimum sampling results, multiple relationships among sampling rates should be of integral powers of 2. To change sampling rates not changed by adjusting A/D converter operating frequency, we used a high-speed complex programmable logic device (CPLD) to calculate the derivative of the lightning signal and determined whether to store current-sampled data base on the results.

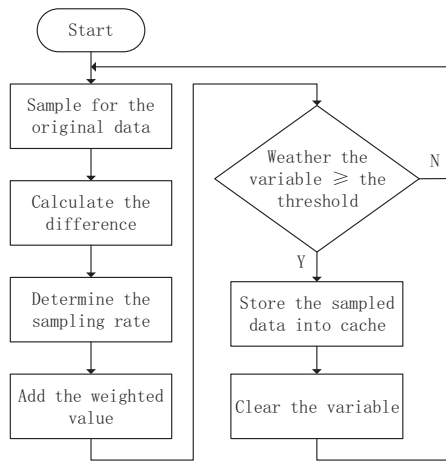


Fig. 4. Work flow chart of the multirate sampled method.

Using the sampling flowchart in Fig. 4, start by sampling original data. Section 3.2 in this paper presents time-frequency analysis of lightning signals. The valuable frequency components of signals are known to commonly be below 1 MHz. Based on the Nyquist theory, lightning currents should be sampled at a sampling rate of more than twice the maximum frequency of the signal. In engineering applications, this rate is generally set at 4 to 16 times higher. Because an excessive rate would increase system costs, however, it is appropriate to sample lightning signals at 6 MHz. Furthermore, the CPLD calculates the difference between adjacent data sampled by the A/D converter as the derivative of the lightning signal at that moment. The processor determines whether to store current sampled data based on the derivative. The peak current of lightning signals varies over a wide range and does not change the frequency distribution inside the waveform, the criterion for choosing the sampling rate should be determined by the maximum derivative of the whole signal, which appears at the wave front based on the time-frequency distribution shown in Section 3.2, to eliminate the influence of peak current on the algorithm. The processor then stores data in the cache as a valid sampling point, when 6 MHz is used, to be the sampling rate at this moment.

In contrast, sampled data is not valid when a lower sampling rate is used, so the processor temporarily stores data for the next calculation. To simplify computing, a weighting summation should be the crux of the algorithm.

Algorithm sequences are as follows: First, define a variable and initialize it at 0. Next, add the value of this variable and a weighted value determined by the result after each calculation for the difference. The sum will be stored back to replace the original variable. When the value of the new variable equals or exceeds the threshold, the processor stores sampling data and clears the variable to complete sampling. For example, assume that we define the threshold as 4. When the sampling rate is chosen to be 6 MHz, value of the variable increases 4.

When the value equals the threshold, the processor

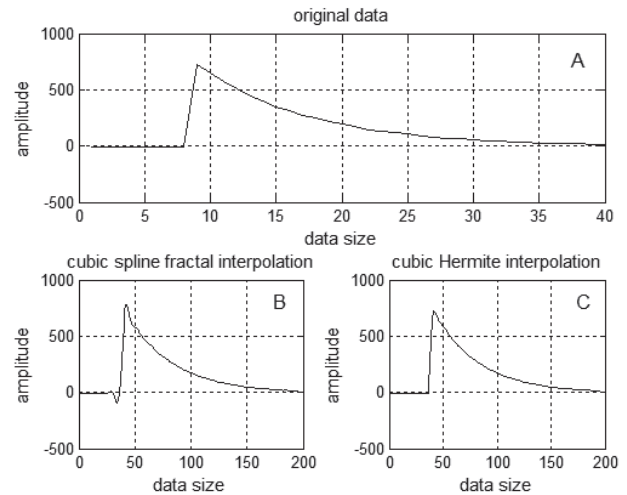


Fig. 5. Comparison of cubic Hermite interpolation and cubic spline fractal interpolation.

completes one sampling and clears the variable. When the sampling rate is 3 MHz, for example, value of the variable increases 2. But if the value is less than the threshold, the processor waits for the next processing cycle. The weighted value should be defined as an integral power of 2 to meet the requirements of the sampling rates mentioned ahead.

3.4. Interpolation

Sequences sampled by using the multirate sampled method are nonuniform. Most methods in frequency spectrum analysis and transformation are mainly for uniform sequences. In contrast, nonuniform sequences have uncontinuity in the time domain, so they will cause high side lobes in the frequency domain if sequences are transformed directly by using the IDFT [21], so they contain many shortcomings in application and may even be harmful to signal processing system's performance. Reconstruction algorithms for nonuniform sequences, for example, are complex, specific and sensitive to noise [22, 23], so transforming nonuniform sequences into uniform sequences is necessary. Here we use piecewise cubic Hermite interpolation to complete this transformation.

The aim of piecewise cubic Hermite interpolation is to transform sequences sampled at a low sampling rate into sequences sampled at a higher sampling rate. Interpolated sequences are uniform. Because sampling agrees with the Nyquist theory, frequency aliasing does not arise. From Eq. (4), we inferred that interpolation performance is good and has high precision, satisfying most sampling requirements.

In addition, the cubic spline fractal interpolation is another common interpolation [24]. Compared with the piecewise cubic Hermite interpolation, cubic spline fractal interpolation has third-order derivative continuity, so it has more oscillations. Fig. 5 shows that the results of interpolating with cubic Hermite interpolation is closer to the source signal than that with cubic spline fractal in-

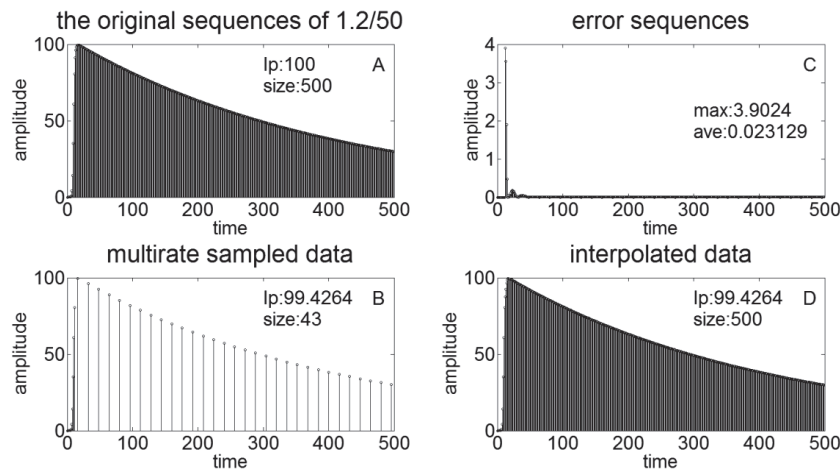


Fig. 6. Simulation test of 1.2/50.

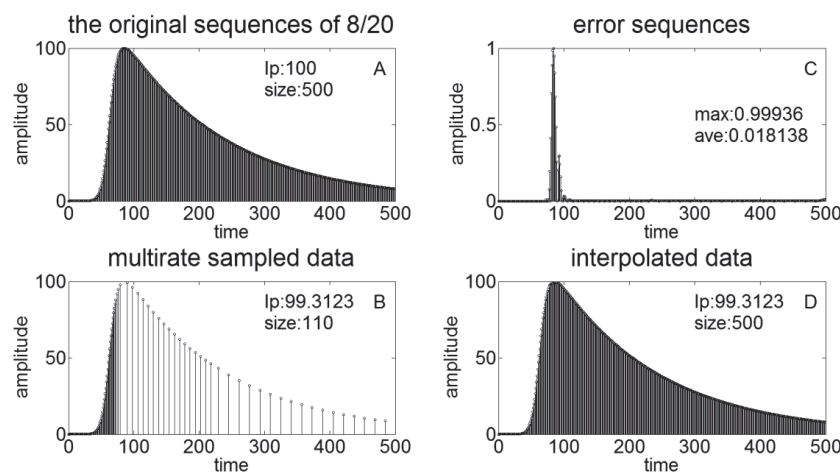


Fig. 7. Simulation test of 8/20.

terpolation, and that cubic spline fractal interpolation has more oscillations and suffers great distortion. This makes it preferable to use piecewise cubic Hermite interpolation.

4. Practical Testing and Simulation

4.1. Simulation

Using MATLAB, we simulated multirate sampling tests of 1.2/50 and 8/20. We first generated typical lightning current waves of 1.2/50 or 8/20 by using the formula in Eq. (7), then simulated sampling of the lightning signal with 6 MHz to get the original lightning sequences. We next applied the multirate sampling method to obtain multirate sampled data. Then we interpolated sampled sequences with cubic Hermite interpolation to get interpolated sequences. Last, we compared interpolated sequences to original data, and calculated the difference between them to get error sequences. To verify the effectiveness of the multirate sampled method, we used the ratio of multirate sampled data to original data to estimate the reduction of redundancy; mean absolute error and variance

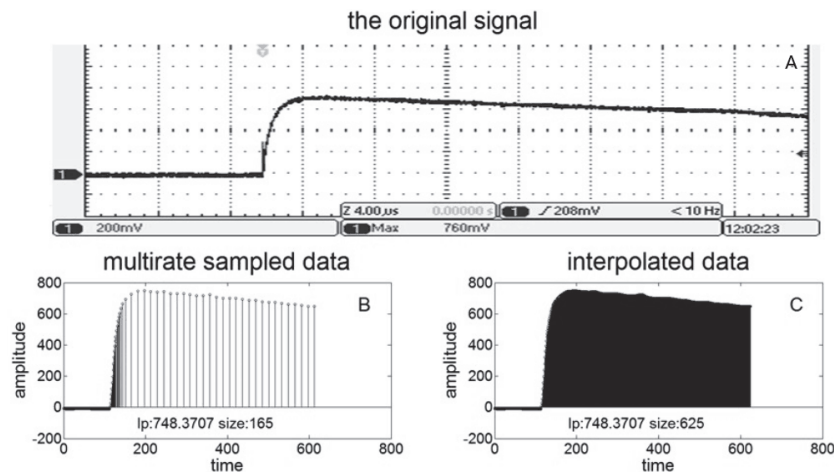
of absolute error sequences are used to estimate accuracy. Simulations results are shown in Figs. 6 and 7.

In the simulation test of 1.2/50, we got the original sequences, whose peak current was 100, by sampling the signal with 6 MHz, containing 500 points. Multirate sampled sequences contain 43 sampling points, reducing the amount of data to about 8.6% of what it originally was. The maximum absolute error of interpolated sequences was 3.9024, the mean absolute error was 0.0231, and variance of absolute error sequences was 0.0633. In the simulation test of 8/20, we also got original sequences, whose peak current was 100, by sampling the signal with 6 MHz, containing 500 points. Multirate sampled sequences contain 110 sampling points, reducing the amount of data to about 22% of the original. The maximum absolute error of interpolated sequences was 0.9994 and the mean absolute error was 0.0181 and variance of absolute error sequences variance was 0.0120.

We simulated these two types of signals by using different amplitudes; test results are shown in Table 2, where I_p is the peak current. Note that the redundancy and accuracy of this method are independent of the signal am-

Table 2. Simulation results.

| Signal | Reduction | Mean | Variance |
|----------------------|-----------|--------|----------|
| $I_p = 100, 1.2/50$ | 8.6% | 0.0231 | 0.0633 |
| $I_p = 500, 1.2/50$ | 8.6% | 0.1163 | 1.5999 |
| $I_p = 1000, 1.2/50$ | 8.6% | 0.2313 | 6.3293 |
| $I_p = 100, 8/20$ | 22% | 0.0181 | 0.0120 |
| $I_p = 500, 8/20$ | 22% | 0.0907 | 0.2994 |
| $I_p = 1000, 8/20$ | 22% | 0.1814 | 1.1977 |

**Fig. 8.** Results of practical tests.

plitude, but the more rapidly the signal changes, the more that redundancy is reduced. But probably, the precision is decreasing simultaneously. Even so, all results show that the multirate sampled method reduced redundancy by about 70%, with lower mean and variance of absolute errors. This means that there is little difference between actual and sampled data.

4.2. Practical Tests

For further verification, we used the impulse current waveform of 1.2/50 for practical tests. **Fig. 8** shows test results. The oscilloscope shows the original wave. Note that the peak current of this original wave is 760 mV. Multirate sampled sequences contain 165 sampling points, reducing the amount of data to about 26.4% of the original. Interpolated sequences, whose peak current is 749 mV, contain 625 points. The maximum absolute error is 11 mV and the waveform rebuilt by the transform coincides with the waveform of the original signal.

5. Conclusions

We have analyzed the frequency distribution of standard lightning signals with the DFT and STFT, and deduced the theoretical basis of the multirate sampled method for lightning current. We found a sampling algorithm and completed piecewise cubic Hermite interpo-

lation by MATLAB to optimize sampled data. Simulation and practical test results have shown that the multirate sampled method effectively reduces redundancy while providing high accuracy. By changing the sampling rate based on variation of the lightning waveform, we could adjust the number of data adaptively to prevent redundant storage. In other words, a higher sampling rate is chosen to assure the integrity of sampling when the lightning signal changes quickly. Otherwise, we would choose a lower sampling rate to reduce redundancy. The size of the data amount no longer need depend on signal sampling time but, instead, on information content, enabling us to use less memory space to store more signals.

In conclusion, the multirate sampled method greatly reduces the consumption of memory resources, i.e., by at least 70%, while helping ensure high accuracy.

Acknowledgements

We gratefully acknowledge the support of the National Key Scientific Instrument and Equipment Development Project (China) under Contracts 2012YQ09016701 and 2011YQ14015006.

References:

- [1] T. Ushio, T. Wu, and S. Yoshida, "Review of recent progress in lightning and thunderstorm detection techniques in Asia," *Atmospheric Research.*, Vol.154, pp. 89-102, 2015.
- [2] C. A. Charalambous, N. Kokkinos, and N. Christofides, "A simulation tool to assess the lightning induced over-voltages on dc cables

- of photo voltaic installations," 2014 Int. Conf. on Lightning Protection (ICLP), CA, Charalambous, China, pp. 1571-1576, 2014.
- [3] S. Okabe, T. Tsuboi, and J. Takami, "Analysis of aspects of lightning strokes to large-sized transmission lines," *IEEE Trans. on Dielectrics and Electrical Insulation*, Vol.18, pp. 182-191, 2011.
- [4] V. A. Rakov and F. Rachidi, "Overview of recent progress in lightning research and lightning protection," *IEEE Trans. on Electromagnetic Compatibility*, Vol.51, pp. 428-442, 2009.
- [5] C. Weijiang, C. Jiahong, G. U. Shanqiang, and Q. Guanjun, "Key technologies of lightning detection and protection in China power grid," *High Voltage Engineering*, Vol.34, pp. 2009-2015, 2008.
- [6] D. Linnan, Y. Zhangqing, and P. Long, "Development and application of multi-channel lightning current on-line monitoring system," *Electric Power*, Vol.48, pp. 59-54, 2015.
- [7] Z. J. Yang and S. Jiang, "Design of lightning detection system based on ARM," 2014 Int. Conf. on Lightning Protection (ICLP), pp. 346-350, 2014.
- [8] C. G. Yao, Y. Long, and H. Wu, "A novel lightning current monitoring system based on the differential-integral loop," *IEEE Trans. on Dielectrics and Electrical Insulation*, Vol.20, pp. 1247-1255, 2013.
- [9] W. A. Chisholm and K. L. Cummins, "Lightning parameters: A review, applications and extensions," *IEEE Trans. on Power Delivery*, Vol.20, pp. 346-358, 2006.
- [10] F. Koehler and J. Swingler, "Simplified Analytical Representation of Lightning Strike Waveshapes," *IEEE Trans. on Electromagnetic Compatibility*, Vol.58, pp. 153-160, 2016.
- [11] R. G. Baraniuk, "Compressive sensing," *IEEE Signal Processing Magazine*, Vol.24, pp. 118-120, 2007.
- [12] L. Durak and O. Arkan, "Short-time Fourier transform: two fundamental properties and an optimal implementation," *IEEE Trans. on Signal Processing*, Vol.51, pp. 1231-1242, 2003.
- [13] F. T. S. Yu and G. W. Lu, "Short-time Fourier transform and wavelet transform with Fourier-domain processing," *Applied Optics*, Vol.33, pp. 5262-5270, 1994.
- [14] M. Zeinali, S. Shahmorad, and K. Mimia, "Hermite and piecewise cubic Hermite interpolation of fuzzy data," *J. of Intelligent and Fuzzy Systems*, Vol.26, pp. 2889-2898, 2014.
- [15] "IEC 61312-1:1995 Protection against lightning electromagnetic impulse-part 1: general principles," Geneva, IEC, 1995.
- [16] W. Xueliang, L. Xuechun, H. Xiaoyan, and S. Yajing, "Analysis of the spatial and temporal distribution characteristics of the cloud-ground lightning in Hubei area," *Meteorological Monthly*, Vol.36, pp. 91-96, 2010.
- [17] W. Juan and C. Yun, "Analysis of the 2009-2012 lightning distribution characteristics in China," *Meteorological Monthly*, Vol.41, pp. 160-170, 2015.
- [18] P. Novak and H. Kyznarova, "Climatology of lightning in the Czech Republic," *Atmospheric Research*, Vol.100, pp. 318-333, 2011.
- [19] V. A. Rakov, A. Borghetti, and C. Bouquegneau, "CIGRE technical brochure on lightning parameters for engineering applications," 2013 Int. Symp. on Lightning Protection (XII SIPDA), Belo Horizonte, BRAZIL: IEEE, pp. 373-377, 2013.
- [20] J. L. Jiang, H. C. Chang, C. C. Kuo, and C. K. Huang, "Transient overvoltage phenomena on the control system of wind turbines due to lightning strike," *Renewable Energy*, Vol.57, pp. 181-189, 2013.
- [21] P. Babu and P. Stoica, "Spectral analysis of non-uniformly sampled data - a review," *Digital Signal Processing*, Vol.20, pp. 359-378, 2010.
- [22] M. W. Maciejewski, H. Z. Qui, and I. Rujan, "Nonuniform sampling and spectral aliasing," *J. of Magnetic Resonance*, Vol.199, pp. 88-93, 2009.
- [23] L. Jinchao, D. Zhaoxiang, and J. Yanjun, "Spectrum analysis and weak signal detection based on nonuniform sampling," *J. of Data Acquisition & Processing*, Vol.27, pp. 320-326, 2012.
- [24] A. K. B. Chand and P. Viswanathan, "Cubic Hermite and cubic spline fractal interpolation functions," 2012 Numerical Analysis and Applied Mathematics (ICNAAM), Kos, Greece: ESCMSET, pp. 1467-1470, 2012.



Name:
Xing Jin

Affiliation:
School of Automation, China University of Geosciences

Address:

388 Lumo Road, Hongshan District, Wuhan 430074, China

Brief Biographical History:

2004- Professor, China University of Geosciences



Name:
Dian Zhang

Affiliation:
School of Automation, China University of Geosciences

Address:

388 Lumo Road, Hongshan District, Wuhan 430074, China

Brief Biographical History:

2014- Graduate Student, China University of Geosciences



Name:
Jingjing Zhang

Affiliation:
School of Automation, China University of Geosciences

Address:

388 Lumo Road, Hongshan District, Wuhan 430074, China

Brief Biographical History:

2014- Assistant Professor, China University of Geosciences



Name:
Yuan Feng

Affiliation:
School of International Education, Changchun Institute of Technology

Address:

395 Road Kuanping, Chaoyang district, Changchun 130012, China